

Milli-Joule pulses post-compressed from 14 ps to 475 fs in bulk-material multi-pass cell based on cylindrical vector beam

Xu Zhang(张旭), Zhaohua Wang(王兆华), Xianzhi Wang(王羡之), Jiawen Li(李佳文), Jiajun Li(李佳俊), Guodong Zhao(赵国栋), and Zhiyi Wei(魏志义)

Citation: Chin. Phys. B, 2023, 32 (**10**): 104206. DOI: 10.1088/1674-1056/acd5c6
Journal homepage: http://cpb.iphy.ac.cn; http://iopscience.iop.org/cpb

What follows is a list of articles you may be interested in

Nonlinear perturbation of a high-order exceptional point: Skin discrete breathers and the hierarchical power-law scaling

Hui Jiang(江慧), Enhong Cheng(成恩宏), Ziyu Zhou(周子榆), and Li-Jun Lang(郎利君)
Chin. Phys. B, 2023, 32 (**8**): 084203. DOI: 10.1088/1674-1056/accb47

High power, widely tunable femtosecond MgO:PPLN optical parametric oscillator

Jinfang Yang(杨金芳), Chong Wang(王翀), Weijun Ling(令维军), Jingwen Xue(薛婧雯), Xiaojuan Du(杜晓娟), Wenting Wang(王文婷), Yuxiang Zhao(赵玉祥), Feiping Lu(路飞平), Xiangbing Li(李向兵), Jiajun Song(宋贾俊), Zhaohua Wang(王兆华), and Zhiyi Wei(魏志义)
Chin. Phys. B, 2023, 32 (**7**): 074204. DOI: 10.1088/1674-1056/accd59

Two-photon absorption of $FAPbBr_3$ perovskite nanocrystals

Xuanyu Zhang(张轩宇), Shuyu Xiao(肖书宇), Xiongbin Wang(王雄彬), Tingchao He(贺廷超), and Rui Chen(陈锐)
Chin. Phys. B, 2023, 32 (**6**): 064212. DOI: 10.1088/1674-1056/acb203

Numerical investigation of the nonlinear spectral broadening aiming at a few-cycle regime for 10 ps level Nd-doped lasers

Xi-Hang Yang(杨西杭), Fen-Xiang Wu(吴分翔), Yi Xu(许毅), Jia-Bing Hu(胡家兵), Pei-Le Bai(白培乐), Hai-Dong Chen(陈海东), Xun Chen(陈洵), and Yu-Xin Leng(冷雨欣)
Chin. Phys. B, 2022, 31 (**9**): 094206. DOI: 10.1088/1674-1056/ac685e

Sensitive absorption measurements of hydrogen sulfide at 1.578 μm using wavelength modulation spectroscopy

Xia Hua (夏滑), Dong Feng-Zhong (董凤忠), Wu Bian (吴边), Zhang Zhi-Rong (张志荣), Pang Tao (庞涛), Sun Peng-Shuai (孙鹏帅), Cui Xiao-Juan (崔小娟), Han Luo (韩荦), Wang Yu (王煜)
Chin. Phys. B, 2015, 24 (**3**): 034204. DOI: 10.1088/1674-1056/24/3/034204

Milli-Joule pulses post-compressed from 14 ps to 475 fs in bulk-material multi-pass cell based on cylindrical vector beam

Xu Zhang(张旭)[1,2], Zhaohua Wang(王兆华)[1,2,3,†], Xianzhi Wang(王羡之)[1], Jiawen Li(李佳文)[1,2], Jiajun Li(李佳俊)[1,2], Guodong Zhao(赵国栋)[1,2], and Zhiyi Wei(魏志义)[1,2,3,‡]

[1] *Beijing National Laboratory for Condensed Matter Physics, Institute of Physics, Chinese Academy of Sciences, Beijing* 100190, *China*
[2] *University of Chinese Academy of Sciences, Beijing* 100049, *China*
[3] *Songshan Lake Materials Laboratory, Dongguan* 523808, *China*

(Received 29 April 2023; revised manuscript received 12 May 2023; accepted manuscript online 16 May 2023)

A cylindrical vector beam is utilized to enhance the energy scale of the pulse post-compressed in a bulk-material Herriott multi-pass cell (MPC). The method proposed here enables, for the first time to the best of our knowledge, pulse compression from 14 ps down to 475 fs with throughput energy beyond 1 mJ, corresponding to a compression ratio of 30, which is the highest pulse energy and compression ratio in single-stage bulk-material MPCs. Furthermore, we demonstrate the characteristic of the vector polarization beam is preserved in the MPC.

Keywords: cylindrical vector beam, post-compression, multi-pass cell

PACS: 42.65.–k, 42.65.Re, 42.60.–v **DOI:** 10.1088/1674-1056/acd5c6

1. Introduction

Ultrafast and ultra-high intensity laser pulses are used today in numerous disciplines ranging from fundamental science to industrial processing, spectroscopy, medical science, and so on. Major scientific achievements within ultrafast science always rely on the cutting-edge laser source technology, which pushes forward the development of lasers with higher parameters. In particular, it is of great challenge to improve peak and average power simultaneously, and many advanced technologies have been applied in this field. The broadband Ti:sapphire lasers, which have been prevailing since the 1990s for sub-50-fs pulse durations and high-intensity applications, are gradually replaced by laser architectures with less emission bandwidth but better average power scalability, most prominently by ytterbium-doped lasers.[1–3] So far, most applications mentioned above employ Ti:sapphire or ytterbium-doped femtosecond amplifiers. The pulse energy of femtosecond lasers based on Ti:sapphire or Yb-doped gain media has reached a high level by using the chirped pulse amplification (CPA) technology.[4,5] All kinds of costly dispersive elements like chirped mirrors, Gires–Tournois mirrors, transmission reflection gratings and chirped fiber Bragg gratings are normally employed in CPA systems, which greatly increase the complexity and cost of the laser systems. However, the mode-locked Nd:YVO_4 oscillators can generate 10 ps pulses without dispersive elements, which can be amplified to hundreds of micro-Joules or even several milli-Joules directly without the CPA technology, exhibiting the advantages of low cost and compact configuration.[6] Thus, compressing picosecond pulses to obtain femtosecond laser pulses with pulse energy of hundreds of micro-Joules by post-compression technology becomes meaningful work.

Pulse post-compression technology is the combination of nonlinear spectral broadening and dispersion compensation. Various spectral broadening methods have been commonly applied, including nonlinear propagation within the bulk material,[7] single or multi-plates,[8–11] hollow-core photonic crystal fibers,[12] slab waveguide,[13,14] multiple focusing in gas medium,[15] and multi-pass cells (MPCs).[16–20] The MPC method offers high efficiency, high-power handling, excellent beam quality, and large compression ratios while being easily adaptable to a large variety of laser pulse parameters including durations ranging currently from 10 ps to a few cycles[17] as well as pulse energies ranging from a few μJ to more than 100 mJ.[18,20]

The energy scale of MPCs is limited by the damage threshold of the cavity mirrors and nonlinear medium. Especially, the Kerr lens effect causes self-focusing, which aggravates damage to the material, due to the characteristics of the Gaussian mode distribution. Longer MPC devices can be used to obtain a larger volume of eigenmode for higher energy throughput. However, even for an almost 8-m-long chamber with noble gas as the nonlinear medium, the output energy still could not exceed tens of milli-Joules. In 2021, Kaumanns *et al.* demonstrated a new method to enhance the energy scale to 112 mJ in gas MPC,[18] through the use of the first-order vortex optic field which is the helical Laguerre–Gaussian mode with the donut-like transverse intensity distribution. The helical Laguerre–Gaussian mode can degrade the peak intensity

†Corresponding author. E-mail: zhwang@iphy.ac.cn
‡Corresponding author. E-mail: zywei@iphy.ac.cn

© 2023 Chinese Physical Society and IOP Publishing Ltd

and weaken self-focusing to avoid optical damage, not only by the bigger spot but also by the hollow transverse intensity distribution. This process is irrelevant to the vortex phase of the helical Laguerre–Gaussian mode, insensitive to the vortex term $e^{i\varphi}$. It is feasible for other plane wavefront modes which have a similar transverse distribution, such as cylindrical vector beams.

In this work, we experimentally exploit cylindrical vector beams for the energy scaling of an MPC and demonstrate the characteristics of cylindrically symmetric polarization maintained in the spectrum broadening. We present the post-compression of the milli-Joule scale pulse and show the compressibility from 14 ps to 475 fs. This corresponds to the highest energy and the highest compression ratio in single-stage bulk-material MPC systems, to our best knowledge.

2. Experimental setup

The layout of the experimental setup of the picosecond laser MPC post-compression device is shown in Fig. 1.

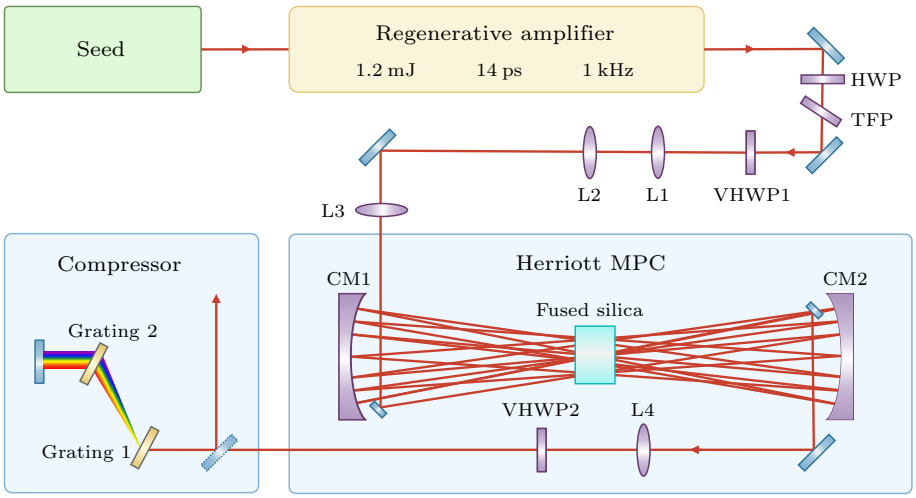


Fig. 1. Scheme of the experimental setup. VHWP1 and VHWP2 denote the vortex half-wave plates, Lens1–3 and Lens4 are substitutes for the input mode matching and out-put collimation optical systems, CM1 and CM2 are the concaves with 300 mm of radius of curvature.

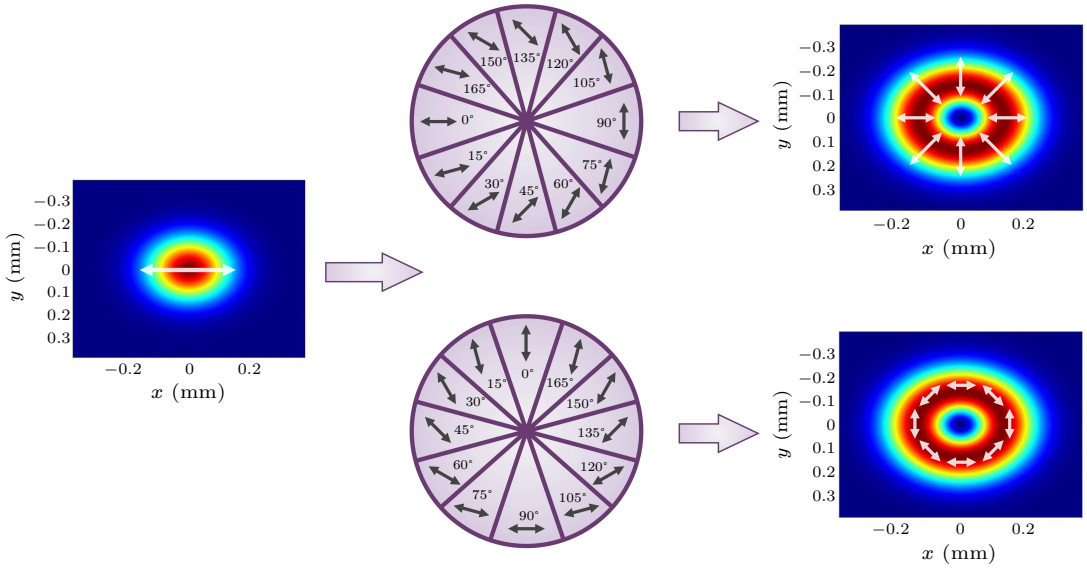


Fig. 2. Scheme of generation of a cylindrical vector beam using a vortex half-wave plate, and the transverse distribution of polarization. Upper: the radial polarization beam. Lower: the azimuthal polarization beam.

A Nd:YVO_4 regenerative amplifier is employed as the driving laser. The 8 ps pulses with a repetition rate of 68 MHz at the central wavelength of 1064 nm generated by the oscillator is used as seed, directly injected into the 1 kHz regenerative amplifier. The pulse energy is amplified to 1.3 mJ and the pulse duration is stretched to 14 ps due to the gain narrowing effect. The spectrum full width at half maximum (FWHM) of the picosecond driving laser is 0.26 nm.

A half-wave plate (HWP) and thin-film polarizers (TFPs) control the input energy into the post-compression device. The linear polarization driving laser is converted to a first-order cylindrical vector polarization beam by placing an op-

tical vortex half-wave plate VHWP1 with a topological charge of $l = +1$, which is composed of multiple 1064 nm half-wave plates whose fast axes rotate at a certain angle in turn, as shown in Fig. 2. The polarization state varies with the polar angle in polar coordinates, and at the center of the beam is a topological singularity, causing a donut-like intensity pattern as shown in Fig. 2. Rotate the half-wave vortex plate to acquire the radial polarization beam or the azimuthal polarization beam.

The beam is approximately modulated to LG_{10} mode, which has the distribution[16]

$$LG_{lm} = LG_{00}\left(\frac{\rho}{w}\right)^{|l|} L_m^l\left(\frac{2\rho^2}{w^2} e^{i\varphi_{lm}(z)}\right). \tag{1}$$

For $l = m = 0$ the distribution also reduces to the fundamental Gaussian beam solution LG_{00}, L_m^l is the associated Laguerre polynomials, $\varphi_{lm}(z) = (2m + l + 1)\tan^{-1}(z/z_0)$ is the Gouy phase shift.

The mode of driving laser has been matched, so as to ensure similar nonlinear pulse propagation characteristics for each roundtrip. The mode matching of the picosecond driving laser to the eigenmode of the Herriott type MPC is achieved by using a 1:2 Galilean telescope system (L1, L2) and a focusing plano-convex lens (L3, $f = 750$ mm).

The Herriott-type MPC consists of two concave cavity mirrors CM1 and CM2 (CM508-150-E03, Thorlabs). The diameter and radius of curvature of two concave cavity mirrors are 3 inches and 300 mm, respectively. The distance between two concave cavity mirrors is set to be about 500 mm.

A fused silica bulk material with thickness of 25 mm and diameter of 2 inches is employed as the Kerr medium, which provides nonlinear boarding of the spectrum by the effect of the self-phase modulation (SPM). Both end faces of the fused bulk silica are coated with anti-reflection coating at the central wavelength of 1064 nm. The fused bulk silica is placed at the waist of the MPC cavity.

The driving laser coupling in and out of the MPC is realized by two mini rectangular mirrors. Round trip times between two concave cavity mirrors of the driving laser can be adjusted by finely tuning the cavity length of the MPC. The driving laser is aligned to pass through 56 roundtrips inside the MPC cavity in our experiment, which corresponds to 111 times passing through the Kerr medium. This process broadens the spectrum of driving picosecond laser by the SPM, which makes it support a shorter Fourier transform-limited (FTL) pulse duration. The overall length of the driving laser propagating in the medium is much less than the dispersion length for the picosecond pulse, so it is unnecessary to consider the material dispersion, and it can be assumed that the duration of the driving laser is constant. It is required to compensate for the residual dispersion to obtain a shorter pulse.

A second vortex half-wave plate VHWP2 identical to the first vortex half-wave plate VHWP1 is placed into the beam after the beam is coupled out of the MPC device. By rotating the orientation of the VHWP2 to the corresponding angle, the phase delay is compensated for, and the output beam is converted to vertical polarization to acquire higher diffraction efficiency of the grating.

Finally, a pair of transmission gratings is set for removing the positive chirp introduced by the SPM effect and the fused-silica material dispersion, which is 1000 line/mm and optimized for vertical polarization. The laser is incident on the gratings at a Littrow angle of 32.1° after collimated by Lens4.

3. Experimental results

We calculate the distribution of the MPC cavity Gaussian eigenmode by *ABCD* matrix, the diameter of the MPC cavity Gaussian eigenmode of 1064 nm is 0.96 mm and 0.388 mm on the concave cavity mirrors and in the waist of the MPC device, respectively. The beam waist of Laguerre–Gaussian mode is $\sqrt{M^2}$ times larger than the Gaussian eigenmode LG_{00}, scales as

$$w_{LG_{lm}} = \sqrt{M^2} w_{\text{eigen}}. \tag{2}$$

For Laguerre–Gaussian mode $M^2 = 2m + |l| + 1$, the diameter of the corresponding first-order cylindrical vector beam LG_{10} is 1.36 mm and 0.55 mm on the concave cavity mirrors and in the waist of the MPC device, respectively.

Experimentally, when injecting the MPC with a Gaussian beam, the maximum throughput energy is 370 μJ, which is limited by the self-focusing and damage threshold of the coating and the fused silica.

Due to the LG_{10} mode distribution of the cylindrical vector beam, the peak power intensity attenuates 2.7 times.[20] Moreover, the donut-like beam distribution significantly weakens the self focusing. Thus, with cylindrical vector beam, the maximum input energy increases to more than 1.3 mJ, which is about 3.7 times higher than that of the Gaussian beam.

For robustness considering mode matching errors, mirror imperfections, or the development of hot spots in the beam, the input energy is set to 1.2 mJ. The output pulse energy after MPC post-compression increases linearly with the increase of the input pulse energy adjusted by the combination of half-wave plate and thin-film polarizer, which implies that there are only linear losses in the MPC post-compression. Finally, the output energy of the MPC device is 1.03 mJ, corresponding to a transmission efficiency of 86%. The loss mainly stems from reflection loss.

We measured the polarization state intensity distribution of the beam through a rotatable linear polarizer under different orientations before and after the MPC device, respectively.

Figures 3(a) and 3(c) show the azimuthal polarization beam distributions before and after the MPC, respectively. Figures 3(b) and 3(d) present the radial polarization beam distributions before and after the MPC, respectively. The top left-hand corner of each figure is the intensity distribution of the beam without the polarizer, and the other three part is the corresponding intensity distributions after the polarizer. The output beam is still a clean doughnut mode in Figs. 3(b) and 3(d) and the polarization state intensity distribution of the output beam is the same as the corresponding input beam. It is demonstrated that polarization is not affected by self-phase modulation in the MPC. The MPC device is a polarization preserving system.

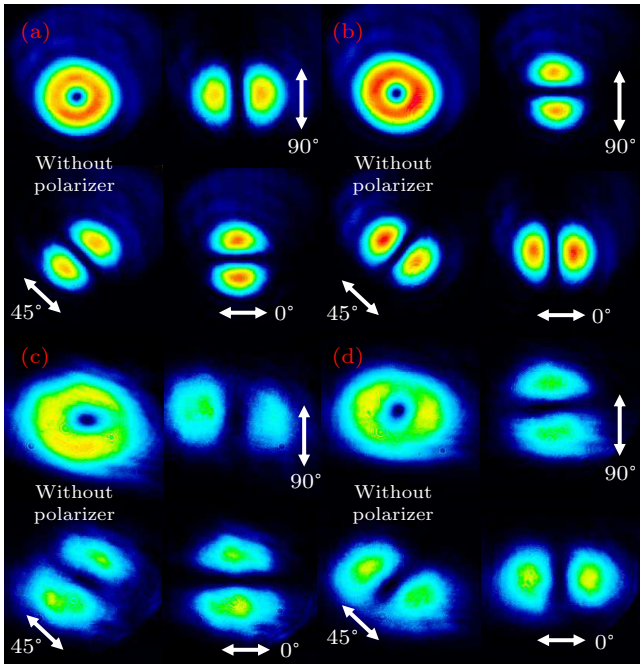


Fig. 3. The polarization intensity distribution of the input and output beams measured by a linear polarizer. (a) and (b) The profiles of input azimuthal polarization and radial polarization beam, respectively. (c) and (d) The profiles of the corresponding output azimuthal polarization and radial polarization beam, respectively.

Figure 4 depicts the measured spectrum before VHWP2, the measured spectrum is broadened by the MPC device, and spanning from 1059 nm to 1069 nm. When we rotate the VHWP1 to convert the radial polarization to the azimuthal polarization, the measured spectrum does not vary with it, which demonstrates that the SPM process in the MPC is insensitive to the polarization state once more.

The shape of broadened spectrum approximately follows the expected profile of self-phase modulation known from the MPC with a linear polarization beam. The central peak is a consequence of the background, which is the part of 68 MHz seed, non-amplified and recorded by the spectrometer at low-frequency mode.

The Fourier-transform limit of the measured broadened spectrum is 456 fs. After a pair of transmission gratings, -3.2×10^{-6} fs^2 GDD is provided to remove the chirp and to compress the pulse duration. A shortest intensity autocorrelation trace signal of 637 fs is measured by a commercial intensity autocorrelator (PulseCheck-50, A. P. E. GmbH), as shown in Fig. 5. The intensity autocorrelation function deconvolution factor of the FTL pulse is 0.746, assuming that the deconvolution factor of the compressed pulses is the same as the FTL pulses. Therefore, the duration of compressed pulses is 475 fs, which is slightly longer than that of the FTL, and may be attributed to the high order dispersion. The compression factor is approximately 30.

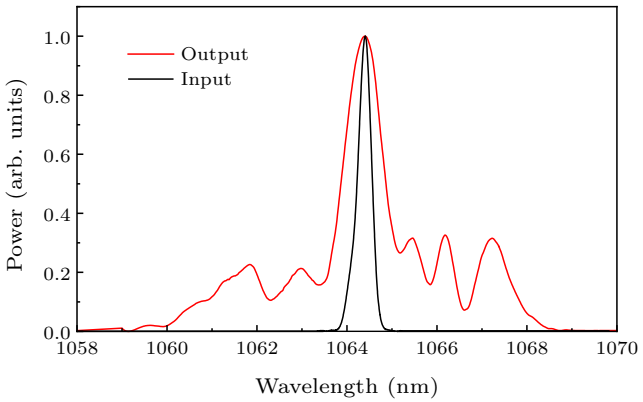


Fig. 4. Measured input (black) and output (red) spectrum.

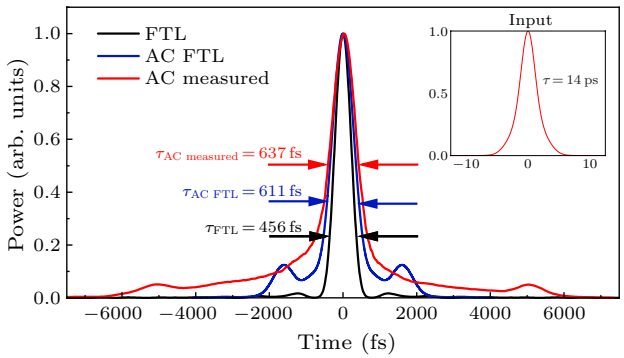


Fig. 5. Fourier limited pulse calculated from the output spectrum shown in Fig. 3 together with the autocorrelation trace calculated for FTL pulse (blue) and the measured autocorrelation trace (red). The measured input pulse and its FWHM duration are shown in the inset.

4. Conclusion

We have demonstrated the post-compression in a bulk-material multi-pass cell (MPC) with output energy 1 mJ pulse, significantly improving the energy scale of bulk-material MPCs by converting a linear polarization input beam to a first-order cylindrical vector polarization beam. The pulse duration is compressed from 14 ps down to 475 fs, corresponding to a compression ratio of 30. To the best of our knowledge, this work is the highest pulse energy output from the MPC with the bulk material as the nonlinear medium. Moreover, this is the highest pulse compression ratio in single-stage bulk-material MPCs. We demonstrate that the characteristic of vector polarization beam is preserved in the process of spectral broadening

in the MPC, no matter what is the donut-like transverse distribution or the polarization state. There is still great potential of pulse post-compression energy scale with higher order vector polarization beams.

References

[1] Mukhin I B, Volkov M R, Vikulov I A, Perevezentsev E A and Palashov O V 2020 *Quantum Electron.* **50** 321

[2] Yan D Y, Liu B W, Chu Y X, Song H Y, Chai L, Hu M L and Wang C Y 2019 *Chin. Opt. Lett.* **17** 4

[3] Jauregui C, Limpert J and Tünnermann A 2013 *Nat. Photon.* **7** 861

[4] Calendron A L, Cankaya H and Kartner F X 2014 *Opt. Express* **22** 24752

[5] Sung J H, Lee H W, Yoo J Y, Yoon J W, Lee C W, Yang J M, Son Y J, Jang Y H, Lee S K and Nam C H 2017 *Opt. Lett.* **42** 2058

[6] Yoon J W, Kim Y G, Choi I, Sung J H, Lee H W, Lee S K and Nam C H 2021 *Optica* **8** 630

[7] Nagy T, Simon P and Veisz L 2021 *Adv. Phys. X* **6** 1845795

[8] Cao H B, Nagymihaly R S, Khodakovskiy N, Pajer V, Bohus J, Lopez-Martens R, Borzsonyi A and Kalashnikov M 2021 *Opt. Express* **29** 5915

[9] Kim J I, Yoon J W, Yang J M, Kim Y G, Sung J H, Lee S K and Nam C H 2022 *Opt. Express* **30** 26212

[10] Zhu B B, Fu Z Y, Chen Y D, Peng S N, Jin C, Fan G Y, Zhang S, Wang S J, Ru H, Tian C S, Wang Y H, Kapteyn H, Murnane M and Tao Z S 2022 *Opt. Express* **30** 2918

[11] Zhang S, Fu Z Y, Zhu B B, Fan G Y, Chen Y D, Wang S J, Liu Y X, Baltuska A, Jin C, Tian C S and Tao Z S 2021 *Light: Sci. Appl.* **10** 53

[12] Emaury F, Saraceno C J, Debord B, Ghosh D, Diebold A, Gerome F, Sudmeyer T, Benabid F and Keller U 2014 *Opt. Lett.* **39** 6843

[13] Hamster H, Sullivan A, Gordon S, White W and Falcone R W 1993 *Phys. Rev. Lett.* **71** 2725

[14] Arnold C L, Zhou B, Akturk S, Chen S, Couairon A and Mysyrowicz A 2010 *New J. Phys.* **12** 073015

[15] Tsai M S, Liang A Y, Tsai C L, Lai P W, Lin M W and Chen M C 2022 *Sci. Adv.* **8** eabo1945

[16] Viotti A L, Seidel M, Escoto E, Rajhans S, Leemans W P, Hartl I and Heyl C M 2022 *Optica* **9** 197

[17] Rueda P, Videla F, Witting T, Torchia G A and Furch F J 2021 *Opt. Express* **29** 27004

[18] Kaumanns M, Pervak V, Kormin D, Leshchenko V, Kessel A, Ueffing M, Chen Y and Nubbemeyer T 2018 *Opt. Lett.* **43** 5877

[19] Song J, Wang Z, Lv R, Wang X, Teng H, Zhu J and Wei Z 2021 *Appl. Phys. B* **127** 50

[20] Kaumanns M, Kormin D, Nubbemeyer T, Pervak V and Karsch S 2020 *Opt. Lett.* **46** 929